Large optical third-order nonlinearities in a switchable Prussian blue analogue

Amine Ould-Hamouda, Antonio Iazzolino, Hiroko Tokoro, Shin-Ichi Ohkoshi, Eric Freysz

Large optical third-order nonlinearities in a switchable Prussian blue analogue

AMINE OULD-HAMOUDA,[1] ANTONIO IAZZOLINO,[1] HIROKO TOKORO,[2,3] SHIN-ICHI OHKOSHI,[2] AND ERIC FREYSZ[1]*

[1]*Univ. de Bordeaux, CNRS- UMR 5798, LOMA- UMR 5798, 351 Cours de la Libération, 33405 Talence Cedex, France*
[2]*Department of Chemistry, School of Science, The university of Tokyo, 7-3-1 Hongo, Bunko-ku, Tokyo 113-0033, Japan*
[3]*Division of Materials Science, Faculty of Pure and Applied Sciences, University of Tsukuba, 1-1-1, Tennodai, Tsukuba, Ibaraki 305-8573, Japan*
**eric.freysz@u-bordeaux.fr*

Abstract: We report on the observation of an efficient coherent up-conversion via third harmonic generation (THG) in $Rb_{0.94}Mn[Fe(CN)_6]_{0.98}.0.3H_2O$ material. Our THG measurements at fundamental wavelengths ranging from 1200 to 2400 nm show that, in this spectral range, the THG signal overcomes the signal generated by frequency doubling. This demonstrates that this material possesses significant third-order nonlinear optical (NLO) responses. Its effective $\chi^{(3)}$ value is at least two orders of magnitude greater than α-Quartz. We also demonstrate that this material exhibits a broad thermal hysteresis loop around room temperature, which makes it possible to simultaneously photo-commute its linear and third-order nonlinear optical properties.

OCIS codes: (190.0190) Nonlinear optics; (160.4330) Nonlinear optical materials; (160.6840) Thermo-optical materials; (160.2900) Optical storage materials.

References and links

1. A. Ludi, H. U. Güdel, Struct. Bonding (Berlin) **14**, 1–21 (1973).
2. S. Ohkoshi, S. Saito, T. Matsuda, T. Nuida, H. Tokoro, "Continuous Change of Second-order Nonlinear Optical Activity in a Cyano-bridged Coordination Polymer," J. Phys. Chem. C **112**(34), 13095–13098 (2008).
3. H. Tokoro, S. Ohkoshi, "Continuous change of second-order nonlinear optical activity in a cyano-bridged coordination polymer photo-induced phase transition in RbMnFe Prussian blue analog-based magnet," in *Chemical, biological, and nanophotonic technologies for nano-optical devices and systems*, Otsu Motoichi, ed. (Springer, Berlin, 2010).
4. Y. R. Shen, *The principles of nonlinear Optics* (Wiley, 1984).
5. R. W. Boyd, *Nonlinear optics*, (Academic Press, 2008).
6. P. N. Butcher, D. Cotter, *The element of nonlinear optics*, (Cambridge, 1990).
7. S. Ohkoshi, T. Nuida, T. Matsuda, H. Tokoro, K. Hashimoto, "The dielectric constant in a thermal phase transition magnetic material composed of rubidium manganese hexacyanoferrate observed by spectroscopic ellipsometry," J. Mater. Chem. **15**, 3291–3295 (2005).
8. S. K. Kurtz, T. T. Perry, "A powder techniques for the evaluation of nonlinear optical materials," J. Appl. Phys. **39**, 3798-3813 (1968).
9. I. Aramburu, J. Ortega, C. L. Folcia, J. Etxebarria, "Second-harmonic generation in dry powders: A simple experimental method to determine nonlinear efficiencies under strong light scattering," Appl. Phys. Letters, **104**, 071107-1-071107-4 (2014).
10. I. Aramburu, J. Ortega, C. L. Folcia, J. Etxebarria,"Second-harmonic generation by micropowders: A revision of the Kurtz–Perry method and its practical application," Appl. Phys. B **116**(1), 211–233 (2014).
11. M. Liu, H. S. Quah, S. Wen, Z. Yu, J. J. Vittal, W. Ji, "Efficient third harmonic generation in a metal−organic framework," Chem. Mater. **28**(10), 3385−3390 (2016).
12. D. N. Christodoulides, I. C. Khoo, G. J. Salamo, G. I. Stegeman, and E. W. Van Stryland, "Nonlinear refraction and absorption: mechanisms and magnitudes," Advances in Optics and Photonics **2**, 60–200 (2010).
13. X. Yang, S. Xie," Expression of third-order effective nonlinear susceptibility for third-harmonic generation in crystals," Appl. Optics **34**(27), 6130–6135 (1995).

14. $E \sim \sqrt{\frac{2Z_0 I}{\tau S}}$ where I, Z_0, τ and S are the energy of the pulse, the impedance of free space (~377 ohms), the pulse duration and surface of the laser beam on the sample, respectively.
15. G. Galle, J. Degert, C. Mauriac, C. Etrillard, J.F. Letard, E. Freysz, "Nanosecond study of spin state transition induced by a single nanosecond laser shot on $[Fe(NH_2trz)_3]$ compounds inside and outside their thermal hysteresis loops," Chem. Phys. Lett. **500**(1–3), 18–22 (2010).

1. Introduction

Cyano-bridged coordination polymers composed of $-M_A$-NC-M_B- (M_A and M_B are transition metal ions), Prussian blue analogs, have the centrosymmetric face centered cubic structure of $M_A^{II}[M_B^{III}(CN)_6]_{2/3}$ z H_2O [1]. When an alkali (A) ion is inserted during the synthesis, Prussian blue analogs take on the $A^I M_A^{II}[M_B^{III}(CN)_6]$-type structure. It has been recently shown that above x=0.7, such a polymer of $Rb_xMn[Fe(CN)_6]_{(x+2)/3}$ z H_2O displays a structural change between a cubic centrosymmetric $m\bar{3}m$ structure to a cubic noncentrosymmetric $\bar{4}3m$ structure [2]. The latter phenomenon has been demonstrated by recording the evolution of X-ray powder diffraction versus Rb content as well as by recording the second-harmonic generation (SHG) signal emitted when exciting a sample with nanosecond Nd:YAG pulses centered at λ=1.064 μm [2]. Above x=0.7, the SHG signal has been shown to steadily increase with the content of Rb. However, regardless of the content of Rb, the second-order optical susceptibility of this material remains small and is about one order of magnitude smaller than α-Quartz. Moreover, this material is photo-switchable and presents a large thermal hysteresis loop at room temperature, thus offering many other prospects, e.g., in the recording of optical data [3]. Indeed, for x=0.94, when the temperature is decreased from T=320 K to T=240 K, one records a phase transition from a light brown noncentrosymmetric cubic ($\bar{4}3m$) to a dark brown noncentrosymmetric tetragonal ($\bar{4}m2$) space group. As shown in Fig. 1, this phase transition displays a broad thermal hysteresis loop, which is recorded between T~300 K and T~200 K. Since both space groups are noncentrosymmetric, an SHG signal can be recorded in both phases. However, the amplitude of the SHG signal is different in the cubic and tetragonal phases.

As a general rule, in condensed matter, the amplitude of nonphase-matched second-order nonlinear effects (such as SHG) overcomes the amplitude of nonphase-matched third-order nonlinear phenomena (such as third-harmonic generation (THG)) [4-6]. Hereafter, we report on an efficient nonphase-matched THG in a noncentrosymetric $Rb_{0.94}Mn[Fe(CN)_6]_{0.98}.0.3H_2O$ crystal powder, and study its evolution versus the excitation wavelength at different temperatures of the sample. The THG signal is found to be very large, visible with the naked eye, and largely overcoming the simultaneously generated nonphase-matched SHG signal, indicating that under our experimental conditions $\chi^{(3)}E>\chi^{(2)}$. The measured effective third-order value, we labeled $\chi^{(3)}_{RbMnFe}$ hereafter, is found to be ~5×10^{-20} $m^2.V^{-2}$, more than two orders of magnitude larger than α-Quartz, which is ~3.6×10^{-22} $m^2.V^{-2}$ over a broad spectral range. This has to be compared to the $\chi^{(2)}_{RbMnFe}$ susceptibility previously reported for this material ($\chi^{(2)}_{123}$~0.032 $pm.V^{-1}$), which is about an order of magnitude smaller than α-Quartz ($\chi^{(2)}_{111}$(Quartz)~0.7 $pm.V^{-1}$) [2]. Moreover, we will demonstrate that one can also record a photo-induced phase transition in this system, which makes it possible to modulate the amplitude of the THG signal. This clearly indicates our ability to photo-control the effective third-order optical nonlinearity of this material.

2. Experimental methods

2.1 Material preparation and characterization

The samples' preparation has been previously published [2]. The prepared samples of $Rb_{0.94}Mn[Fe(CN)_6]_{0.98}.0.3H_2O$ consisting of cubic micro-crystals with a size of 2.1±0.7 µm. For the measurements, a powder of $Rb_{0.94}Mn[Fe(CN)_6]_{0.98}.0.3H_2O$ was inserted in between the microscope slide and cover slide, gently pressed, and heated at 330 K. As displayed in Fig. 1, when the temperature is decreased from T=330 K to T= 200 K, the color of this sample changes from light brown to dark brown.

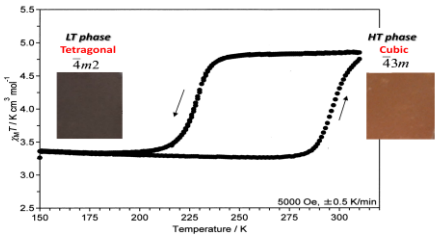

Fig. 1: Hysteresis loop of the sample revealed by the χ_MT-T plots. The insets show that in the LT phase the color of the sample is dark brown. Its color turns light brown in the HT phase.

The XRD patterns and Rietveld analyses indicate that the change of color is related to the switching of the micro-crystallites from a cubic $\bar{4}3m$ structure, hereafter called the high-temperature (HT) phase, to a tetragonal $\bar{4}m2$ structure, hereafter referred to as the low-temperature (LT) phase. Moreover, as displayed in Fig. 1, this phase transition displays a broad thermal hysteresis loop that is recorded in between ~300 K and 200 K. The evolution of the absorption and refractive index of this material measured in the visible and near IR spectral range in both the LT and HT phases and deduced from previously reported spectroscopic ellipsometry measurements are presented in Fig. 2 [7]. The evolution of the refraction index and the absorption coefficient of the sample in the LT and HT phases in the 1.1–2.4 µm spectral range were estimated by extrapolating with a polynomial fit the data obtained in the 600–800 nm spectral range. This approximation is valid, considering that the sample is weakly absorbing in the 1–2.4 µm spectral range. In the HT phase, one can notice the presence of a broad absorption peak centered at ~460 nm, which is likely due to the intervalence transfer band from the Mn^{III}-NC-Fe^{II} to Mn^{II}-NC-Fe^{III} and Jahn–Teller distorted Mn^{III}. In the LT phase, this absorption peak is shifted toward ~410 nm and its amplitude decreases. The latter absorption has been assigned to the ligand-to-metal charge transfer (LMCT) transition of the $[Fe^{III}(CN)_6]$.

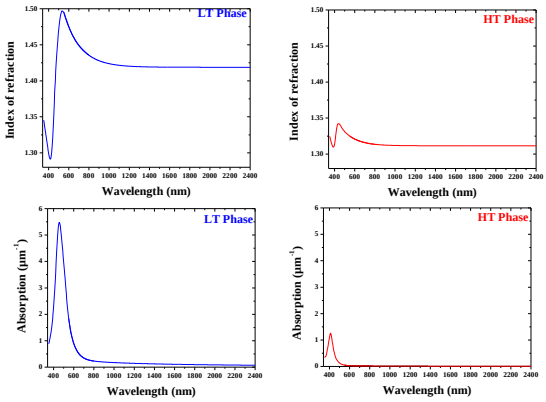

Fig 2: Absorption spectra and refractive indices of the sample in the LT and HT phases (deduced from [S. Ohkoshi et al., J. Mater. Chem. 15, 3291–3295 (2005).]).

2.2 THG experiments

The experimental set-up we used to perform our experiments is presented in Fig. 3. The sample was excited by 160 femtosecond pulses yielded by an optical parametric amplifier (OPA), which has a central wavelength that can vary from 1100–2400 nm. At the exit of the OPA, an infrared (IR) glass filter is inserted. It transmits the IR pulses produced by the OPA and blocks the visible light produced within this system. The laser pulse is then slightly focused over a beam waist of 235 µm onto the sample, and its maximal energy is 1.5 µJ. The THG signal generated at the surface of the sample was than collimated and focused on the entrance slit of spectrometer. In front of this spectrometer, another colored glass filter was used. The latter transmits the visible light and blocks the infrared excitation pulse. A thermally cooled charge coupled detector (CCD) is used to record the spectrum at the exit of the spectrometer.

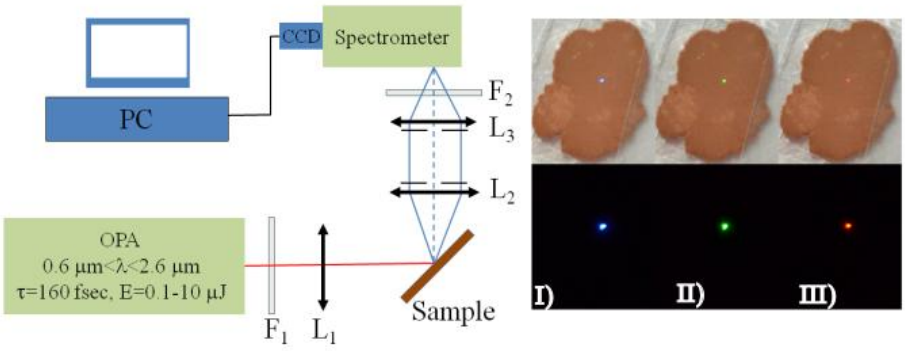

Fig.3: THG experimental set-up and pictures of the THG signal produced at the surface of the sample when excited by femtosecond pulses centered at I) λ=1400 nm, II) λ=1600 nm and III) λ=1900 nm.

3. Results and discussion

The THG signal is easily visible with the naked eye. Photographs of the THG signal produced at the surface of the sample in room light and in the dark are displayed in Fig. 3. These photographs are taken in the HT phase, at a temperature T=290 K, when the sample is excited by OPA pulses whose central wavelength is fixed to λ=1400 nm Fig. 3(I), λ=1600 nm Fig. 3(II) and λ=1900 nm Fig. 3(II), respectively. The sample is held in a thermally controlled

cold finger in which the temperature is set at T=290 K. To switch the sample from the LT phase to the HT phase, it is heated for several minutes at T=330 K and then slowly cooled down to T=290 K. During this process, the color of the sample changes from dark brown to light brown. To bring the sample from the HT phase to the LT phase, it is cooled for several minutes by means of a nitrogen jet and slowly heated back to T=290 K, as displayed in Fig. 1. This also results in a change in the color of the sample from light brown to dark brown .

The evolution of the THG signal in the LT and HT phases versus the power of the excitation pulse centered at λ=1920 nm is displayed in Fig. 4(a). In both the LT and HT phases, the intensity of the THG signal exhibits cubic power dependence. Moreover, regardless of the excitation intensity, the spectrum of the THG signal in the LT phase, displayed in the inset of Fig. 4(a), is found to be in very good agreement with the spectrum of the excitation pulses.

The normalized spectra of the THG signal recorded in the HT phase when one tunes the central wavelength of the excitation pulses from λ=1.2 µm to λ=2.4 µm are presented in Fig. 4(b). Almost identical results are recorded in the LT phase. This figure, along with Fig. 3, indicates that one can easily record a THG signal over the entire visible spectral range. As mentioned previously, our sample also exhibits a second-order optical nonlinear effect. We therefore have simultaneously record SHG and THG signals. However, in agreement with the pictures presented in Fig. 3, the amplitude of the THG signal is found to be at least one order of magnitude larger than the SHG signal.

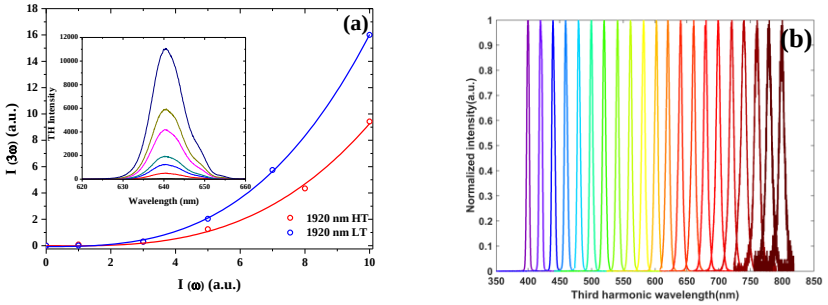

Fig. 4: a) Evolution of the spectra and intensity of THG signal versus the intensity at the fundamental wavelength. The experiment was performed in the LT and HT phases exciting the sample at λ=1920 nm. b) Normalized THG spectra recorded at different excitation wavelengths.

Regardless of the excitation wavelength we used, we could not detect the THG signal at the back surface of the sample. Therefore, the THG signal we record has to be generated at the air-sample interface or very near the surface of the sample. As indicated in Fig. 5(a), two different physical phenomena could give rise to this signal. At first, the THG signal may be directly generated by the surface of the sample within the surface coherence length $L_{c,s}=\pi/(k(3\omega)+3k(\omega))$, where $k(3\omega)$ and $k(\omega)$ are the wave-vectors at the fundamental and third harmonic frequencies, respectively. Since the theory for THG in the limit of weak pump depletion is the same as for SHG, the irradiance of this THG signal writes $I_s(3\omega) \propto L_{c,s}^2 \left[\chi_{RbMnFe}^{(3)}\right]^2 I^3(\omega)$ where $\chi_{RbMnFe}^{(3)}$ is the effective susceptibility of our sample and I(ω) is the light irradiance at the fundamental frequency ω [8–10]. Note that, due to the very small value of $L_{c,s}$ (<0.1 µm), the absorption of the THG signal within this length interval can be neglected. Second, the THG signal may also be directly generated in the volume of the sample over the coherence length $L_{c,v}=\pi/(k(3\omega)-3k(\omega))$. However, when the size of crystallites r is smaller than $L_{c,v}$ ($L_{c,v}>r>> L_{c,s}$), the irradiance of the THG signal is only generated within the size r of the crystallites. Within a single crystallite, the THG signal writes [11]:

$$I_V(3\omega,r) \propto r^2\left[\chi^{(3)}_{RbMnFe}\right]^2 \frac{sin^2\left(\frac{\Delta kr}{2}\right)+sinh^2\left(\frac{\alpha r}{4}\right)}{\left(\frac{\Delta kr}{2}\right)^2+\left(\frac{\alpha r}{4}\right)^2} e^{-\alpha r/2} I^3(\omega) \quad (1)$$

Where Δk=k(3ω)-3k(ω) is the wave-vector mismatch, α the absorption coefficient at 3ω, and I(ω) is the light irradiance at ω within the crystallites. This volume THG signal is then reflected at the interface between the particles. Then, before reaching the detector, it has to propagate back through the crystallites. Therefore, the THG signal writes: $I_{R,V}(3\omega) = R(3\omega)e^{-\alpha r} I_V(3\omega,r)$, where R(3ω) is the reflection coefficient at the air-crystallites interface. The latter expression neglects the very small contribution of the THG signal generated by the fundamental beam reflected at the exit interface of micro-crystallites. At normal incidence, R(3ω) writes: $R(3\omega) = \frac{(n-1)^2+\kappa^2}{(n+1)^2+\kappa^2}$, where n and k are the real and imaginary parts of the index of refraction at 3ω, respectively. To discriminate between the volume ($I_{R,V}(3\omega)$) and surface ($I_s(3\omega)$) contribution, we have evaluated the ratio $I_s(3\omega)/I_{R,V}(3\omega)$, and as expected, we found that regardless of the excitation wavelength, $I_s(3\omega)$ is always at least an order of magnitude smaller than $I_{R,V}(3\omega)$. In the next section of this paper, we will therefore ignore the contribution of $I_s(3\omega)$ to the THG signal.

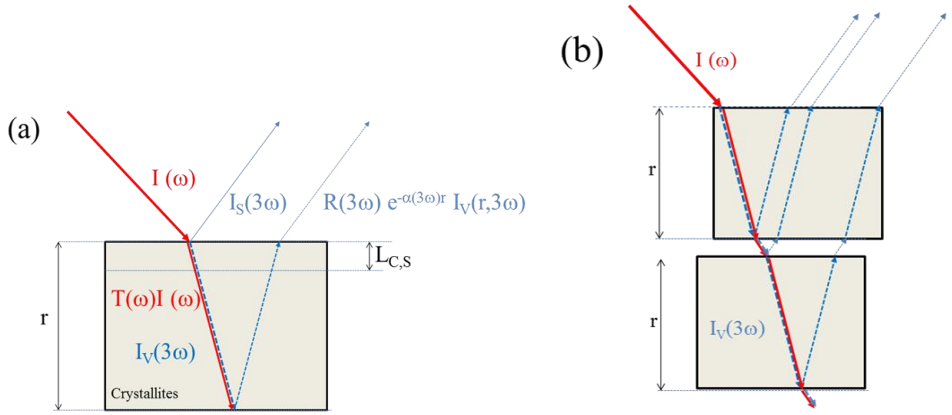

Fig. 5: Micro-crystallite geometry considered for the computation of β

In fact, the THG signal is collected from an ensemble of crystallites. For the crystallites at the bare air-powder interface, the THG signal writes [8–10]:

$$I'_V(3\omega,r) \propto \mathrm{N}\sum I_V(3\omega,r),$$

where N is the number of crystallites per unit surface involved in the THG process. However, as shown in Fig. 5(b), the beam at a fundamental frequency can also reach crystallites beneath this bare interface and generate a THG signal. The THG signals produced within this layer of micro-crystallites also contribute to the overall THG signal. If one only considers the absorption of the THG signal, together with the reflection and transmission of the beam by the crystallites at fundamental, third harmonic frequencies, it can be easily shown that the THG signal produced by M superposed layers of crystallites writes:

$$I_V^T(3\omega,r) \propto \beta(\omega,M)N\sum I_V(3\omega,r)\,, \quad (2)$$

with

$$\beta(\omega,M) = R(3\omega)[1+T^2(3\omega)]\sum_{n=1}^{M} T^{6(n-1)}(\omega)T^{2n-1}(3\omega)e^{-n\alpha r}\,,$$

where T(ω), R(3ω), T(3ω) are the transmission, reflection, and transmission coefficients at the air-crystallite interface at the fundamental and third harmonic frequencies, respectively. Due to the spectral evolution of T(ω), R(3ω), and T(3ω) the behavior of β(ω,M) in the LT and HT phases was found to be almost constant above M=64 and presents some characteristic dispersion. It must be noted that Eq. (2) completely neglects the light scattering induced by the micro-crystallites or the multiple reflection occurring within or in between these micro-crystallites. This latter assumption results in an over-estimation of the THG signal [9,10]. On the contrary, in Eq. (2) we also consider that all micro-crystallites are not in close contact with each other and are separated by a thin air layer. The latter assumption may result in an under-estimation of the THG signal. We will therefore suppose that, on average, this over and underestimation of the THG signal cancels out. The THG signal generated in our sample has been calibrated against the THG signal generated at the surface of a 1-mm-thick ZnSe polycrystalline plate. Thanks to the two small irises placed at the back and in the front of the lenses L_2 and L_3, respectively, our experimental set-up makes it possible to almost perfectly set this ZnSe plate at the position of our sample. A razor blade placed on the top surface of the ZnSe plate was used to block the THG light generated in the bulk and reflected by the back surface of the plate. The THG signal we recorded in this experiment is therefore only generated within the surface coherence length $L_{c,s}^{ZnSe}$ =π/(k_{ZnSe}(3ω)+3k_{ZnSe}(ω)) of the ZnSe particles whose micro-crystallites size distribution is centered around 50–70 µm. Regardless of the excitation wavelength, $L_{c,s}^{ZnSe}$ is always two orders of magnitude smaller than the size of these particles. We can therefore consider that $I^{ZnSe}(3\omega)$ writes:

$$I^{ZnSe}(3\omega) \propto N \sum I_V^{ZnSe}{}_V(3\omega, r) \propto N \sum \left(L_{c,s}^{ZnSe}\right)^2 \left[\chi_{ZnSe}^{(3)}\right]^2 I^3(\omega) \qquad (3)$$

Since the THG signal in our sample and in the ZnSe plate are generated from randomly oriented crystal, one can readily evaluate $\chi_{RbMnFe}^{(3)}$ against $\chi_{ZnSe}^{(3)}$ by computing the square root between the THG signal generated under the same experimental conditions by computing the ratio between Eq. (1) and Eq. (2). From this ratio and knowing $L_{c,s}^{ZnSe}$, the coefficients α, Δk, and R(3ω) for our sample, one can infer $\chi_{RbMnFe}^{(3)}$ in the LT and HT phases, considering $\chi_{ZnSe}^{(3)}$ ~2.65×10^{-19} $m^2.V^{-2}$ is constant over our excitation spectral range.

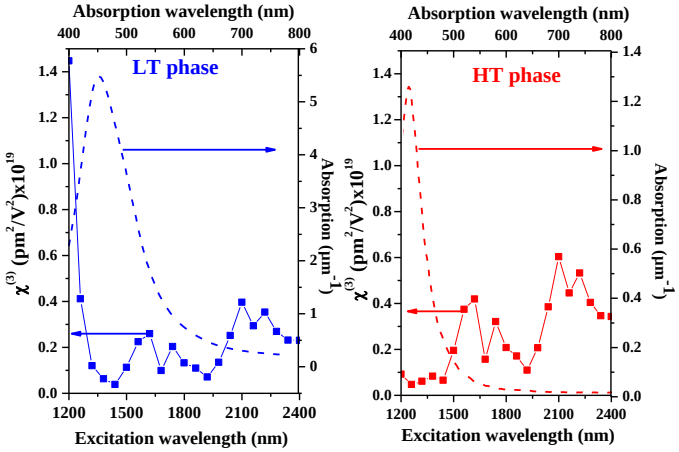

Fig. 6 : Spectral evolution of effective $\chi^{(3)}{}_{RbMnFe}$ and absorption of our sample in the HT (red) and LT (blue) phases. The solid lines are guides for the eyes.

Figure 6 displays the evolution of $\chi_{RbMnFe}^{(3)}$ we computed accordingly, considering that the concentration N of particles in our sample and ZnSe polycrystalline plate are similar. Note that in comparison to ZnSe, the concentration of our very slightly compacted RbMnFe sample

is likely less. Hence, here again we underestimate the value $\chi^{(3)}_{RbMnFe}$. However, in both the LT and HT phases, the values of $\chi^{(3)}_{RbMnFe}$ range between 0.2×10^{-19} m^2 V^{-2} and 1.5×10^{-19} m^2 V^{-2}. These values are smaller but still comparable with $\chi^{(3)}_{ZnSe}$. They are about two orders of magnitude larger than the $\chi^{(3)}$ of α-quartz (~3.6×10^{-22} m^{-2} V^{-2}). However, in the LT phase, as one reaches the excitation wavelength λ=1400 nm, the $\chi^{(3)}_{RbMnFe}$ rapidly increases and reaches a value of ~1.5×10^{-19} m^2 V^{-2} at λ=1200 nm. The latter behavior is likely related to resonant enhancement of the $\chi^{(3)}_{RbMnFe}$ close to the three-photon absorption centered at λ=460 nm. This resonance is not visible in the HT phase. This latter behavior is attributed to the shift of the absorption band toward lower wavelengths in the HT phase as well as the reduction of the absorption peak. However, as illustrated in Fig. 6, the wavelength at which $\chi^{(3)}_{RbMnFe}$ reaches it maximum does not coincide with the three-photon resonant absorption of the sample. It is shifted toward a lower wavelength. This may result from an increase in the absorption of our sample at the fundamental or third harmonic frequency through excited state absorption that is not accounted for by our model [12].

ZnSe adopts a cubic $\bar{4}3m$ structure; therefore, it is optically isotropic. For THG, it exhibits two independent and non-null $\chi^{(3)}$ elements: $\chi^{(3)}_{1111}$ and $\chi^{(3)}_{1212}$. Hence, in our experiment, the crystallites being randomly oriented, we measured an angular average of the THG over these two components, and so is the value of $\chi^{(3)}_{ZnSe}$ in Eq. (3) [8-10].

In the HT phase the $Rb_{0.94}Mn[Fe(CN)_6]_{0.98}.0.3H_2O$ also adopts a cubic $\bar{4}3m$ structure. It therefore also exhibits two independent and non-null $\chi^{(3)}$ elements. Hence, the effective $\chi^{(3)}_{RbMnFe}\ (HT)$ value we measured in our experiment can be readily compared to the effective value of $\chi^{(3)}_{ZnSe}$. However, at an LT, our $Rb_{0.94}Mn[Fe(CN)_6]_{0.98}.0.3H_2O$ sample switches from a cubic to a tetragonal $\bar{4}2m$ structure. For THG, the latter structure exhibits five independent elements: $\chi^{(3)}_{1111} = \chi^{(3)}_{2222}$, $\chi^{(3)}_{3333}$, $\chi^{(3)}_{1133} = \chi^{(3)}_{2233}$, $\chi^{(3)}_{1122} = \chi^{(3)}_{2112}$, $\chi^{(3)}_{3223} = \chi^{(3)}_{3113}$ [13]. The value $\chi^{(3)}_{RbMnFe}\ (LT)$ is here again an angular average over these values, and it cannot be directly compared to the effective value of $\chi^{(3)}_{ZnSe}$.

Knowing the amplitude of $\chi^{(3)}_{RbMnFe}$ and $\chi^{(2)}_{RbMnFe}$ of our sample, one can evaluate the threshold value of electric fields E_{th} for which $\chi^{(3)}E_{th}>\chi^{(2)}$, i.e., the value of E_{th} for which the non-phase matched THG overcomes the non-phase matched SHG. One found $E_{th}\sim\chi^{(2)}_{RbMnFe}/\chi^{(3)}_{RbMnFe}$ ~10^6 V m^{-1}. This computation is valid when the coherence length for SHG and THG are about the same amplitude, which is the case for the sample we studied. This value of E_{th} has to be compared to the amplitude of the electric field associated with our femtosecond laser pulses, which is about two orders of magnitude larger (E~1 10^8 V.m^{-1} for 0.1 μJ and E~4×10^8 V.m^{-1} for 1.5 μJ [14]). Therefore, in agreement with our observations, the electric fields associated with our laser pulses being two orders of magnitude larger than E_{th}, we do expect the nonphase matched THG signal to overcome the nonphase matched SHG signal. Note that this phenomenon will be difficult to evidence in either α-Quartz or ZnSe where $E\sim\chi^{(2)}/\chi^{(3)}$ is expected to be larger than 10^8 V.m^{-1}.

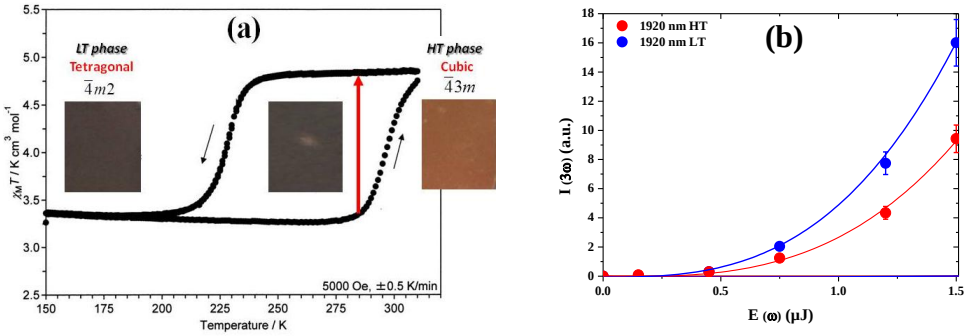

Fig. 7 : a) Pictures of the sample in the LT and HT phases. The central picture displays the sample that has been excited by a powerful laser pulse. The shined spot turns from dark brown to light brown. b) Evolution of the THG signal versus the intensity of the fundamental laser beam. The solid lines in blue and red are the THG signals recorded in the LT and HT phases, respectively. The blue and red dots are the THG signals recorded at low intensity before and after photo-commutation of the sample, respectively.

An interesting property of $Rb_{0.94}Mn[Fe(CN)_6]_{0.98}.0.3H_2O$ is that it is bistable. Hence, within its thermal hysteresis loop that lies in between 225 K and 290 K, it can be set in either the LT or HT phase. Since the value of $\chi^{(3)}_{RbMnFe}$ differs in the two phases, one should be able to simultaneously switch the linear and the nonlinear optical properties of this material. As proof of this concept, we have performed the following experiment. The sample was initially set in the LT phase at 285 K. As mentioned previously, in the LT phase, the color of the sample is dark brown. The THG signal was then recorded, exciting the sample at λ=1920 nm by varying the energy of the exciting pulse in between 0.1 and 1.5 µJ. Afterwards, we increase the energy of the pulse to ~10 µJ. After several seconds, when a sequence of these more powerful pulses was used, as displayed in Fig. 7(a), the color of the area excited by these pulses turned from dark brown to light brown. This indicates the sample is likely switched from the LT phase to the HT phase [3]. To confirm this was indeed the case, we reduced the energy of the laser pulses from 10 µJ to 0.1–1.5 µJ. The THG signals recorded for these lower energies were compared to the THG signals we previously recorded when the sample was set in the HT phase for similar laser energies. As shown in Fig. 7(b), the amplitude of these two THG signals recorded at T=285 K were found to be almost similar. This indicates that indeed we have switched the sample from the LT to the HT phase. Then, the sample was brought back in the LT phase by cooling it with a nitrogen jet. After this process, the sample recovered its dark brown color, and the amplitude of the THG signal was almost identical to the one we recorded at the beginning of this experiment. This experiment was repeated at least ten times for exciting pulses with intensities between 0.1 and 1.5 µJ. Within our experimental uncertainties (± 5%), we effectively reproduced these results. This experimental proof of concept indicates that one is indeed able to photo-switch back and forth the linear and third-order nonlinear optical properties of this sample from the LT phase to the HT phase. To understand the mechanism that gives rise to the photo-switching between the LT to the HT phase, we carried out this experiment reducing the exposure, the exciting pulse repetition rate. We found that the mechanism at the origin of the photo-switching phenomena is likely thermal. In other words, the laser beam power is absorbed and results in an increase in the local temperature of the sample. If the local temperature is strong enough, the area shined by the laser beam is brought from the LT phase to the HT phase. Within the thermal hysteresis loop, it remains in this state and can be switched back to the LT phase by decreasing the temperature of the sample beyond the thermal hysteresis loop [15].

4. Conclusion

In sum, we have observed and measured THG in a powder of $Rb_{0.94}Mn[Fe(CN)_6]_{0.98}.0.3H_2O$. Our THG measurements at fundamental wavelengths ranging from 1100 nm to 2400 nm show that, in this spectral range, the THG signal overcomes the SHG signal. At maximum, the effective $\chi^{(3)}$ value is comparable with that of a ZnSe poly-crystallites wave-plate and is in the 1.2–2.4 μm spectral range at least two orders of magnitude larger than that of α-Quartz. We have also demonstrated that, within its thermal hysteresis loop, the linear and third-order nonlinear optical properties of this material can be photo-switched. This demonstrates the potential of such Prussian blue analogs for nonlinear optical applications.